

# DECI-HERTZ INTERFEROMETER GRAVITATIONAL-WAVE OBSERVATORY: FORECAST CONSTRAINTS ON THE COSMIC CURVATURE WITH LSST STRONG LENSES

SHUO CAO<sup>1\*</sup>, TONGHUA LIU<sup>2</sup>, MAREK BIESIADA<sup>3</sup>, YUTING LIU<sup>1</sup>, WUZHENG GUO<sup>1</sup>, ZONG-HONG ZHU<sup>1†</sup>

*Draft version December 2, 2021*

## ABSTRACT

In this paper, we aim at using the DECI-hertz Interferometer Gravitational-wave Observatory (DECIGO), a future Japanese space gravitational-wave antenna sensitive to frequency range between LISA and ground-based detectors, to provide gravitational-wave constraints on the cosmic curvature at  $z \sim 5$ . In the framework of the well-known distance sum rule, the perfect redshift coverage of the standard sirens observed by DECIGO, compared with lensing observations including the source and lens from LSST, makes such cosmological-model-independent test more natural and general. Focusing on three kinds of spherically symmetric mass distributions for the lensing galaxies, we find that the cosmic curvature is expected to be constrained with the precision of  $\Delta\Omega_K \sim 10^{-2}$  in the early universe ( $z \sim 5.0$ ), improving the sensitivity of ET constraints by about a factor of 10. However, in order to investigate this further, the mass density profiles of early-type galaxies should be properly taken into account. Specially, our analysis demonstrates the strong degeneracy between the spatial curvature and the lens parameters, especially the redshift evolution of power-law lens index parameter. When the extended power law mass density profile is assumed, the weakest constraint on the cosmic curvature can be obtained. Whereas, the addition of DECIGO to the combination of LSST+DECIGO does improve the constraint on the luminosity density slope and the anisotropy of the stellar velocity dispersion significantly. Therefore, our paper highlights the benefits of synergies between DECIGO and LSST in constraining new physics beyond the standard model, which could manifest itself through accurate determination of the cosmic curvature.

*Keywords:* Gravitational waves(678); Strong gravitational lensing (1643); Cosmological parameters (339)

## 1. INTRODUCTION

The question of whether the Universe is spatially open, flat or closed, which can be quantitatively addressed by determining the cosmic curvature parameter (hereafter  $\Omega_k$ ) has been the subject of recent intense discussions. Nowadays, a large amount of independent observations have provided strong evidence supporting the spatial flatness of our Universe within the current precision (Cai et al. 2016; Li et al. 2016c; Wei & Wu 2017; Wang et al. 2017; Rana et al. 2017), which is well consistent with the predictions of different inflationary models (Ichikawa et al. 2006; Virey et al. 2008). However, the recent Planck 2018 results, which provided the latest measurements of temperature and polarization of the cosmic microwave background anisotropy (Aghanim et al. 2018), tend to favor a spatially closed Universe over  $2\sigma$  confidence level ( $\Omega_k = -0.044^{+0.018}_{-0.015}$ ). It should be pointed out that in several recent works (Liu et al. 2019) the validity of the result might be as problematic, due to its strong dependency on the assumed non-flat  $\Lambda$ CDM model. Such tension becomes one of the major puzzles in modern cosmology. On the one hand, the constraints on  $\Omega_k$  also have important consequences for properties of dark energy (Clarkson et al. 2007; Gong & Wang 2007), considering the correlation

between the cosmic curvature and dark energy model used in fitting different observational data, such as the Baryon acoustic oscillation, Hubble parameter, and angular size measurement (Ryan et al. 2019). Others have argued that the derived values of the cosmic curvature are highly dependent on the validity of the background FLRW metric, a more fundamental cosmological assumption which has been investigated in many recent studies with strongly lensed SNe Ia and gravitational waves (Denissenya et al. 2018; Cao et al. 2019a). In any case, in order to better understand the curvature tension and the nature of dark energy, it is necessary to emphasize the importance of determining model-independent measurements of the spatial curvature with different geometrical methods. This could also be reason why providing and forecasting fits on  $\Omega_k$  from current and future astrophysical observations has become an outstanding issue in modern cosmology (Cai et al. 2016; Li et al. 2016c; Wei & Wu 2017; Wang et al. 2017; Rana et al. 2017).

In this paper, we focus on the Distance Sum Rule (DSR) in the framework of strong gravitational lensing (SGL) by early-type galaxies (Takada & Doré 2015; Denissenya et al. 2018; Ooba & Sugiyama 2018). More specifically, the ratios of two angular diameter distance  $D_{ls}/D_s$  (the source-lens/lens distance ratio) can be directly inferred from the observations of Einstein radii, with precise measurements of central velocity dispersions of the lensing galaxies (Bolton et al. 2008; Cao et al. 2012, 2015b). Meanwhile, the distances at redshifts  $z_l$  and  $z_s$  are always measured from several popular distance indicators covering these redshifts, such as SNe Ia, Hubble parameters (Clarkson et al.

<sup>1</sup>Department of Astronomy, Beijing Normal University, 100875, Beijing, China; caoshuo@bnu.edu.cn; zhuzh@bnu.edu.cn

<sup>2</sup>School of Physics and Optoelectronic, Yangtze University, Jingzhou 434023, China;

<sup>3</sup>National Centre for Nuclear Research, Pasteura 7, 02-093 Warsaw, Poland

2008, 2007; Shafieloo & Clarkson 2010; Li et al. 2016c) and intermediate-luminosity radio quasars (Cao et al. 2017a,b) acting as standard candles, cosmic chronometers and standard rulers, respectively. However, the uncertainty of the latest  $\Omega_k$  constraint was quite large due to the limited sample size of available SGL data (Xia et al. 2017; Qi et al. 2019a), focusing on 118 galactic-scale strong lensing systems from the Sloan Lens ACS Survey (SLACS), BOSS emission-line lens survey, Lens Structure and Dynamics, and Strong Lensing Legacy Survey (Cao et al. 2015b). Besides, only a small fraction of the lensing data can be utilized, due to the mismatch of redshifts between the lensing systems (especially the background sources) and the current SNe Ia sample. Such disadvantage of this method will be more severe in the near future, when the source redshift of galactic-scale strong lensing systems is expected to reach  $z \sim 5$  in the forthcoming Large Synoptic Survey Telescope (LSST) (Oguri & Marshall 2010; Verma et al. 2019). Therefore, the direct luminosity distances with high redshifts would significantly contribute to a robust measurement of the cosmic curvature, which has been demonstrated in a recent analysis of UV and X-ray quasars (Risaliti & Lusso 2018).

On the other hand, in the gravitational wave (GWs) domain, one could use the GW signals from inspiralling and merging compact binaries to derive luminosity distances (Schutz 1986). Such methodology has been realized by Advanced LIGO and VIRGO detectors, with the detection of different types of signals including a binary neutron star system (Abbott et al. 2016, 2017). Specially, the Hubble diagram of these so-called standard sirens could be directly constructed and applied in cosmology, with the redshifts measured from their electromagnetic (EM) counterparts. Looking ahead, the next generation detectors like the DECi-Hertz Interferometric Gravitational Observatory (DECIGO), a future Japanese space GW antenna, will extend the detection limit of Advanced LIGO and Einstein Telescope to the earlier stage of the Universe ( $z \sim 5$ ) generating the detections of  $\sim 10^4$  NS-NS binaries per year. In addition, the detection of these binary systems using the second-generation technology of space-borne DECIGO takes place in the inspiral phase long time ( $\sim 5$  years) before they enter the LIGO frequency range, with signal-noise-ratio (SNR) much higher than that of the current and future ground-based GW detectors. Therefore, in this study we propose with the future standard siren sample from DECIGO, the largest compilation of SGL data expected from LSST can be used to infer the cosmic curvature resulting in more precise constraints. This paper is organized as follows. In Sec. 2 and 3, we will briefly introduce the methodology and the simulated data (DECIGO standard sirens and LSST strong lenses) in this analysis. The forecasted constraints on the cosmic curvature are presented in Sec. 4. Finally, we give summaries and discussions in Sec. 5. Throughout the paper, the flat  $\Lambda$ CDM is taken as the fiducial cosmological model in the simulation, with  $\Omega_m = 0.315$  and  $H_0 = 67.4$  km/s/Mpc from the latest *Planck* observations (Aghanim et al. 2018).

## 2. METHODOLOGY

As one of the basic assumptions in cosmology, the cosmological principle (i.e., the Universe is homogeneous

and isotropic at large scales) has been widely applied in different cosmological studies. Now the FLRW metric is introduced to describe the space-time of the Universe (where the speed of light  $c = 1$ )

$$ds^2 = -dt^2 + a^2(t) \left( \frac{1}{1 - Kr^2} dr^2 + r^2 d\Omega^2 \right), \quad (1)$$

where  $K = +1, 0, -1$  denotes the spatial curvature for closed, flat and open geometries, respectively. Note that the curvature parameter is directly related to the constant  $K$  as  $\Omega_k = -k/a_0^2 H_0^2$ . Now we respectively denote the dimensionless comoving distances  $d_l \equiv d(0, z_l)$ ,  $d_s \equiv d(0, z_s)$  and  $d_{ls} \equiv d(z_l, z_s)$ , in the framework of strong lensing system with a source (at redshift  $z_s$ ) observed on the image plane (at redshift  $z_l$ ). Note that the dimensionless comoving distances ( $d$ )

$$d(z_l, z_s) = \frac{1}{\sqrt{|\Omega_k|}} S_K \left( \sqrt{|\Omega_k|} \int_{z_l}^{z_s} \frac{H_0 dz'}{H(z')} \right), \quad (2)$$

where

$$S_K(x) = \begin{cases} \sin(x) & \Omega_k < 0, \\ x & \Omega_k = 0, \\ \sinh(x) & \Omega_k > 0. \end{cases} \quad (3)$$

are connected with the angular diameter distance ( $D_A$ ) as  $d(z_l, z_s) = (1 + z_s) H_0 D_A(z_l, z_s)$ . As was originally proposed in Ratra & Peebles (1988), the distance sum rule in non-flat FLRW models gives

$$d_{ls} = d_s \sqrt{1 + \Omega_k d_l^2} - d_l \sqrt{1 + \Omega_k d_s^2}. \quad (4)$$

with  $d'(z) > 0$  and a one-to-one correspondence between the cosmic time  $t$  and redshift  $z$  (Bernstein (2006)). Such simple relation, which was first used to obtain model-independent measurements of the spatial curvature (Clarkson et al. 2008; Qi et al. 2019a), has also been recently discussed to test the validity of the FLRW metric in the Universe (Qi et al. 2019b) based on different types of gravitational lensing events. Now we could rewrite this fundamental relation so that the strong lensing observations (from LSST lenses) and luminosity distances (from DECIGO standard sirens) are encoded

$$\frac{d_{ls}}{d_s} = \sqrt{1 + \Omega_k d_l^2} - \frac{d_l}{d_s} \sqrt{1 + \Omega_k d_s^2}. \quad (5)$$

The left item can be derived from the source/lens distance ratio  $d_{ls}/d_s = D_{ls}^A/D_s^A$ , based on high-resolution imaging and spectroscopic observations in SGL systems (Cao et al. 2015b).

For a strong lensing system with early-type galaxy acting as intervening lens, one of its typical feature is the Einstein radius ( $\theta_E$ ) depends on the source/lens distance ratio ( $d_{ls}/d_s$ ), the lens velocity dispersion ( $\sigma$ ), and the density profiles of the lens galaxies. Such methodology was originally proposed in Futamase & Yoshida (2001) and extended to different SGL samples (Bolton et al. 2008; Cao et al. 2012, 2015b; Chen et al. 2019), with the aim of quantitatively studying the redshift evolution of cosmic equation of state (Li et al. 2016; Liu et al. 2019), measuring the speed of light at different redshifts (Cao et al. 2018, 2020), and testing the General Relativity at large scale (Cao et al. 2017c; Collett et al. 2018). In this paper, three different models will be included in

our analysis to describe the mass distribution of early-type galaxies: Singular Isothermal Ellipsoid (SIE) lens model, Power-law lens model, and Extended power-law model (Chen et al. 2019; Zhou & Li 2020). If the lens mass profile can be approximately described by SIE, the distance ratio is expressed as (Koopmans et al. 2006)

$$\frac{d_{ls}}{d_s} = \frac{c^2 \theta_E}{4\pi \sigma_{SIE}^2} = \frac{c^2 \theta_E}{4\pi \sigma_0^2 f_E^2}, \quad (6)$$

where  $\sigma_{SIS}$  and  $c$  respectively denote the SIS (Singular Isothermal Sphere) velocity dispersion and the speed of light. The parameter  $f_E$  is introduced to quantify different systematics that could change the observed multiple image separation or generate the difference between  $\sigma_{SIS}$  and the observed velocity dispersion of stars ( $\sigma_0$ ). The relation between the measurement of  $\sigma_0$  from spectroscopy and that estimated from the SIE model has been extensively discussed in Ofek et al. (2003); Cao et al. (2012). In the second case, we take into account a spherically symmetric power-law mass distribution ( $\rho \sim r^{-\gamma}$ ,  $r$  is the spherical radial coordinate from the lens center,) to generalize the simplest Singular Isothermal Sphere lens model, considering the non-negligible deviation from SIS ( $\gamma = 2$ ) based on recent observations of the density profiles of early-type galaxies (Koopmans et al. 2006; Humphrey & Buote 2010; Sonnenfeld et al. 2013a). Now the corresponding distance ratio is rewritten as (Ruff et al. 2011; Koopmans et al. 2006; Bolton et al. 2012)

$$\frac{d_{ls}}{d_s} = \frac{c^2 \theta_E}{4\pi \sigma_{ap}^2} \left( \frac{\theta_{ap}}{\theta_E} \right)^{2-\gamma} f^{-1}(\gamma), \quad (7)$$

where  $f(\gamma)$  is a function of the radial mass profile slope ( $\gamma$ ) and  $\sigma_{ap}$  denotes the projected, luminosity weighted average of the velocity dispersion inside the circular aperture  $\theta_{ap}$  (See Cao et al. (2015b) for the derivation of equivalent  $\sigma_{ap}$  within rectangular apertures). One of the advantages of such power-law lens model is based on the assumption that the distribution of stellar mass follows the same power law as that of the total mass, with the vanishing of velocity anisotropy (Koopmans et al. 2005). Consequently, we take into account these uncertainties by introducing a general mass model for the early-type lens galaxies, with the total (i.e. luminous plus dark-matter) mass density distribution ( $\rho(r) \sim r^{-\alpha}$ ) and the luminosity density profile ( $\nu(r) \sim r^{-\delta}$ ). Here we choose to consider the anisotropy of the stellar velocity dispersion in this analysis, which is quantified by the a new parameter  $\beta(r) = 1 - \sigma_\theta^2/\sigma_r^2$ , where  $\sigma_\theta$  and  $\sigma_r$  are the tangential and radial velocity dispersions, respectively. In the framework of such extended power-law model, the distance ratio can be computed from the radial Jeans equation in spherical coordinate system (Koopmans et al. 2006), by projecting the dynamical mass to the lens mass within the Einstein radius

$$\begin{aligned} \frac{d_{ls}}{d_s} = & \left( \frac{c^2}{4\sigma_{ap}^2} \theta_E \right) \frac{2(3-\delta)}{\sqrt{\pi}(\xi-2\beta)(3-\xi)} \left( \frac{\theta_{ap}}{\theta_E} \right)^{2-\alpha} \\ & \times \left[ \frac{\lambda(\xi) - \beta\lambda(\xi+2)}{\lambda(\alpha)\lambda(\delta)} \right], \end{aligned} \quad (8)$$

where  $\xi = \alpha + \delta - 2$ ,  $\lambda(x) = \Gamma(\frac{x-1}{2})/\Gamma(\frac{x}{2})$ . It is apparent

that this extended power-law model will reduce to the power-law lens model when  $\delta = \alpha$ , i.e., the distribution of stellar mass follows the same power law as that of the total mass.

Combing the above equations with the error propagation formula Eq. (6), we could obtain the uncertainty of SGL systems ( $\sigma_{SGL}$ ) for different lens models, based on the observational uncertainties of the Einstein radius and velocity dispersion. The distance information  $d(z)$  in the right items of Eq. (5) is determined by luminosity distances from gravitational wave data. In this paper, we will present an updated estimation of the cosmic curvature or the FLRW metric from the largest SGL sample by LSST and future GW observations by DECIGO.

### 3. SIMULATIONS FROM DECIGO AND LSST

#### 3.1. Strong lenses from LSST

As one of the most important wide-area and deep surveys besides the Dark Energy Survey (DES) (Frieman et al. 2004), the upcoming Large Synoptic Survey Telescope (LSST) is expected to monitor  $\sim 10^5$  strong gravitational lenses in the most optimistic discovery scenario, by repeatedly scanning nearly half of the sky for ten years (Collett 2015). Such tremendous increase of known galaxy-scale lenses by orders of magnitude will produce extensive cosmological applications in the near future (Cao et al. 2017c, 2018; Ma et al. 2019; Cao et al. 2020). With high-quality imaging and spectroscopic data, the Einstein radius of multiple images and the lens velocity dispersion can be measured precisely and accurately.

In order to assess the performance of forthcoming optical imaging surveys, the simulation of a realistic population of galaxy-galaxy strong lenses has been performed (Collett 2015). The results showed that although  $\sim 10^5$  strong gravitational lenses are discoverable in LSST, only a fraction of SGL sub-sample is available for our curvature estimation, given the expensiveness of substantial follow-up efforts and dedicated spectroscopic observations (spectroscopic velocity dispersion, spectroscopic confirmation of the lens and source redshift) (Hložek et al. 2019). Therefore, in this paper we will simulate a particularly well-selected sub-sample of LSST lenses with the observations of the foreground deflector and the background source population<sup>4</sup>, following the recent analysis of multi-object and single-object spectroscopy to enhance Dark Energy Science from LSST (Mandelbaum et al. 2019). More specifically, it is more realistic to focus only on 5000 well-measured systems with intermediate-mass early-type galaxies acting as strong gravitational lenses, with the velocity dispersion of  $200 \text{ km/s} < \sigma_{ap} < 300 \text{ km/s}$ . Such criteria is strongly supported by the recent findings that for systems with velocity dispersion between 200 km/s to 300 km/s, there is a good consistency between the measurement of  $\sigma_0$  from spectroscopy and those estimated from the SIS lens model (Treu et al. 2006; Cao et al. 2016). In our simulations, we choose the velocity dispersion function (VDF) from DSS Data Release 5 (Choi et al. 2007) to describe the number density of these lensing galaxies, the mass distributions of which are well quantified by

<sup>4</sup> [github.com/tcollett/LensPop](https://github.com/tcollett/LensPop)

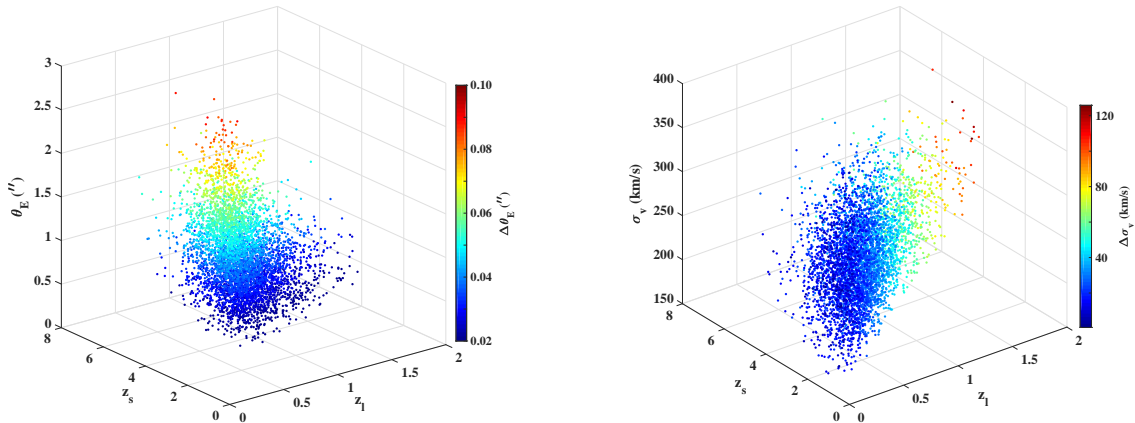


**Figure 1.** The scatter plot of the simulated LSST lensing systems, with the gradient color denoting the uncertainty the Einstein radius and lens velocity dispersion.

the singular isothermal sphere (SIS) model. We take the fractional uncertainty of the Einstein radius and the observed velocity dispersion following the uncertainty budget proposed in Liu et al. (2020).

To assess the analysis of Einstein radius extraction from future LSST survey, some recent attempts have been made to investigate the effect of line-of-sight contamination (Hilbert et al. 2009; Collett & Cunningham 2016), which found that for monitorable strong lenses such effect could introduce a 1-3% uncertainty in the Einstein radius measurements. Such error strategy has been extensively used in the simulation of LSST lens sample, with high-quality (sub-arcsecond) imaging data in general (Cao et al. 2017c). Based on the observations of 32 strong lensing systems from Strong Lensing Legacy Survey (SL2S), with both Canada-France-Hawaii Telescope (CFHT) near-infrared ground-based images or Hubble Space Telescope (HST) imaging data (Sonnenfeld et al. 2013b), Liu et al. (2020) recently investigated the possible anti-correlation between the fractional uncertainty of the Einstein radius ( $\Delta\theta_E$ ) and  $\theta_E$ . The results showed that different error strategies should be applied to strong lenses with different Einstein radii ( $\theta_E$ ), due to the fact that strong lensing systems with smaller  $\theta_E$  will be accompanied with larger statistical uncertainties. Therefore, different from the previous work which took a constant precision for each SGL system observed with HST-like image quality (Cao et al. 2017c), we take 8%, 5% and 3% as the average Einstein radius precision for each system, which could be classified as small Einstein radii lenses ( $0.5'' < \theta_E < 1.0''$ ), intermediate Einstein radii lenses ( $1'' \leq \theta_E < 1.5''$ ), and large Einstein radii lenses ( $\theta_E \geq 1.5''$ ) with HST+CFHT imaging data.

Moreover, Liu et al. (2020) recently proposed that other intrinsic properties of the lensing system (such as the total mass or the brightness of the lensing galaxy) could significantly change the observational precision of lens velocity dispersion. The lessons in the statistical analysis of 70 intermediate-mass lenses (with average velocity dispersion of  $\sigma_{ap} \sim 230$  km/s) observed by Sloan Lens ACS survey (SLACS) (Bolton et al. 2008) showed

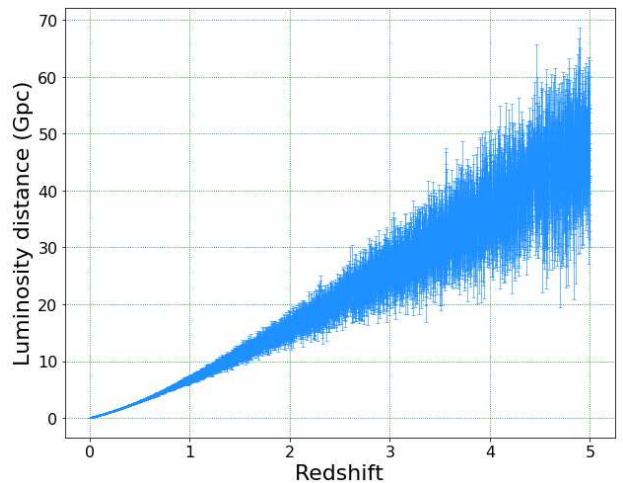


**Figure 2.** The luminosity distance measurements from 10,000 simulated GW events observable by the space detector DECIGO.

the fractional uncertainty is strongly correlated with the lens surface brightness in the  $i$ -band. To incorporate this effect, we consider the anti-correlation between these two quantities and take the best-fitted correlation function obtained in Liu et al. (2020) to simulate the velocity dispersion uncertainty for each LSST lens. Note that such strategy is different from that of the previous work, which assigned an overall error of 5% on each SGL system observed with detailed follow-up spectroscopic information from other ground-based facilities (Cao et al. 2015b; Zhou & Li 2020). The Einstein radius and velocity dispersion distributions of the simulated LSST lenses are plotted in Fig. 1.

### 3.2. Standard sirens from DECIGO

It is well known that GW from inspiraling binaries could provide a new, independent probe of the cosmic expansion using standard sirens (Abbott et al. 2016, 2017). More importantly, the standard siren method, which focuses on binary neutron star mergers coupled with elec-

	$\Omega_k$	$f_E$	$\gamma_0$	$\gamma_1$	$\alpha$	$\delta$	$\beta$
SIS	$0.0001^{+0.012}_{-0.013}$	$1.000^{+0.002}_{-0.002}$	$\square$	$\square$	$\square$	$\square$	$\square$
Power-law spherical	$-0.016^{+0.035}_{-0.037}$	$\square$	$2.001^{+0.001}_{-0.001}$	$0.002^{+0.003}_{-0.003}$	$\square$	$\square$	$\square$
Extended power-law	$-0.007^{+0.050}_{-0.047}$	$\square$	$\square$	$\square$	$2.003^{+0.011}_{-0.011}$	$1.968^{+0.527}_{-0.516}$	$-0.067^{+0.605}_{-0.325}$

**Table 1**

Summary of constraints on the cosmic curvature  $\Omega_k$  and lens model parameters for three types of lens models (See the text for definitions)

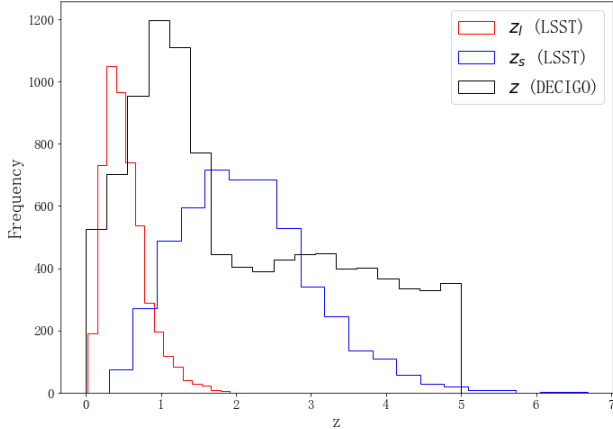


**Figure 3.** Redshift distributions for the GWs from DECIGO, and strong lensing systems (including the source and the lens) from LSST.

tromagnetic (EM) measurements of the redshift, has already been used to produce constraints on the Hubble constant at lower redshift (Zhang et al. 2020), the cosmic opacity and distance duality relation at much higher redshifts (Qi et al. 2019b,c).

Using laser interferometry, the DECi-Hertz Interferometric Gravitational Observatory (DECIGO) is a space mission designed to open the DECi-Hertz frequency range to GW observations (Seto et al. 2001; Kawamura et al. 2011). Compared with the ground-based detectors and other space-based detector such as Laser Interferometric Space Antenna (LISA), DECIGO is expected to detect different populations of GW sources in this unique frequency range of 0.1-1 Hz, including primordial black holes, intermediate-mass black hole binary coalescences, neutron star binary coalescences, and black hole-neutron star binaries in their inspiral phase (Kawamura et al. 2011). The loudest objects in this band of the GW sky are expected to be mergers of neutron star binary coalescences, long time before they enter the LIGO frequency range. Such advantage, which significantly increases the precision of inferences made from chirp signals (Piórkowska-Kurpas et al. 2020), which yield orders of magnitude more candidate standard sirens in the earlier period of the Universe. More specifically, following the recent estimation of Kawamura et al. (2019), DECIGO will bring us the yearly detection of 10,000 NS-NS systems at redshift  $z \sim 5$ , based on the frequency of the binary coalescences given above. Note that although GW may provide us some information about the source redshifts (Messenger & Read 2012; Messenger & Takami 2014), observations of the EM counterparts or host galaxies by ground-based telescopes are still necessary for these expected GW signals (Cutler & Holz 2009). This offers

the exciting possibility we explore: the ability of deep-redshift standard sirens observed by DECIGO to validate or refute the flat geometry inferred by the newest Planck observations.

Following the simulation process by Geng et al. (2020), we generate mock DECIGO NS-NS standard siren observations based on a flat  $\Lambda$ CDM cosmology and assume that their redshift is known. The NS mass distributions is chosen uniformly in  $[1, 2] M_\odot$ . For each coalescing NS-NS system with physical masses ( $m_1$  and  $m_2$ ) and symmetric mass ratio ( $\eta = m_1 m_2 / M_t^2$ ), one could derive the Fourier transform of the GW waveform as

$$\tilde{h}(f) = \frac{A}{D_L(z)} M_z^{5/6} f^{-7/6} e^{i\Psi(f)}, \quad (9)$$

where  $A = (\sqrt{6}\pi^{2/3})^{-1}$  quantifies the geometrical average over NS-NS system's inclination angle, while  $D_L(z)$  denotes the luminosity distance to the source with the redshifted chirp mass of  $M_z = (1+z)\eta^{3/5}M_t$ . As proposed in previous work (Maggiore 2008), the frequency-dependent phase caused by orbital evolution ( $\Psi(f)$ ) can be derived from 1.5 (or higher) post-Newtonian (PN) approximation. For the purpose of uncertainty estimation, different sources of uncertainties are included in our simulation of luminosity distance. On the one hand, focusing only on the inspiral phase of the GW signal, the instrumental uncertainty for a nearly face-on case is given by  $\sigma_{D_{L,GW}}^{inst} = \frac{2D_{L,GW}}{\rho}$ , where  $\rho$  is the combined SNR for the network of space-borne detector and the factor of 2 is included to quantify the maximal effect of the inclination on the SNR (Zhao et al. 2011). On the other hand, the lensing uncertainty caused by the weak lensing is the other crucial point of our idea, due to large scale structure that could potentially bias the results especially at high redshifts (Sathyaprakash et al. 2010). More specifically, following the procedure extensively applied in the literature (Zhang et al. 2020), it was recently proposed that such weak lensing uncertainty could be modeled as  $\sigma_{D_L}^{lens}/D_L = 0.044z$  for the space-based GW detectors (Cutler & Holz 2009). Therefore, the total uncertainty on the luminosity distance is given by

$$\begin{aligned} \sigma_{D_{L,GW}} &= \sqrt{(\sigma_{D_{L,GW}}^{inst})^2 + (\sigma_{D_{L,GW}}^{lens})^2} \\ &= \sqrt{\left(\frac{2D_{L,GW}}{\rho}\right)^2 + (0.05zD_{L,GW})^2}. \end{aligned} \quad (10)$$

With the luminosity distance from the standard sirens, the uncertainty in  $\sigma_{GW}$  can be expressed as a function of  $D_{L,GW}^s$ ,  $D_{L,GW}^l$ ,  $\sigma_{D_{L,GW}}^s$ , and  $\sigma_{D_{L,GW}}^l$  through the error propagation formula [Eq. (5)].

Now the final key question required to be answered is: how to describe the redshift distribution of GW events that can be detected by DECIGO? Given the

analytical fit of DECIGO noise spectrum including the shot noise, the radiation pressure noise and the acceleration noise (Kawamura et al. 2019, 2006; Nishizawa et al. 2010; Yagi & Seto 2011), the simulated luminosity distances from 10,000 standard sirens in DECIGO is presented in Fig. 2, with the redshift distribution follows the form provided by Sathyaprakash et al. (2010); Cutler & Harms (2006); Schneider et al. (2001). We refer to Geng et al. (2020) for more simulation details of DECIGO standard sirens. For a good comparison, Fig. 3 illustrates the perfect redshift coverage of the simulated DECIGO sample, compared with lensing observations including the source and lens from LSST.

#### 4. RESULTS AND DISCUSSION

In this section, we describe the observational constraint on the cosmic curvature using the observational data-set summarized in Sect. 3. In particular, we simultaneously fit the spatial curvature parameter and lens model parameters to the LSST lens sample and luminosity distance data from DECIGO, and find the best-fit of  $\Omega_K$  in the DSR. The statistical quantity  $\chi^2$  is written as

$$\chi^2(\mathbf{p}, \Omega_k) = \sum_{i=1}^N \frac{(\mathcal{D}_{GW}(z_i; \Omega_k) - \mathcal{D}_{SGL}(z_i; \mathbf{p}))^2}{\sigma_{\mathcal{D}}(z_i)^2}, \quad (11)$$

with the two factors contributing to the uncertainty of distance ratio from the observables of the strong lensing systems in LSST and the luminosity distance measurements from standard sirens in DECIGO. We assume that the two uncertainties of LSST lenses and DECIGO standard sirens are uncorrelated and thus they add in quadrature of  $\sigma_D^2 = \sigma_{SGL}^2 + \sigma_{QSO}^2$ . In order to calculate the posterior distribution of the model parameters, we use the Python module emcee<sup>5</sup>, which is an Affine Invariant Markov chain Monte Carlo (MCMC) Ensemble sampler (Foreman-Mackey & Hogg 2013), to survey the posterior distribution in parameter space and to maximize the likelihood function  $\mathcal{L} \sim \exp(-\chi^2/2)$ .

We assume three kinds of spherically symmetric mass distributions (SIS, power-law model, and extended power-law model) for the lensing galaxies in the cosmic curvature analysis. The 1D and 2D marginalized distributions with  $1\sigma$  and  $2\sigma$  confidence level contours for  $\Omega_K$  and relevant lens parameters constrained from the combined LSST+DECIGO data are shown in Fig. 4-6.

In the framework of the simplest SIS model for the first application of the method described above, we obtain the best-fit value of curvature parameter and the corresponding  $1\sigma$  (more precisely 68% confidence level) uncertainties:  $\Omega_K = 0.0001_{-0.013}^{+0.012}$ , which indicates that the cosmic curvature can be accommodated at very high precision ( $\Delta\Omega_K = 10^{-2}$ ) comparable to that derived from the Planck CMB power spectra (Aghanim et al. 2018). Compared with the previous results obtained in Räsänen et al. (2015), the fits on the cosmic curvature have been improved by two orders of magnitudes, benefit from the significant increase of well-measured strong lensing systems and standard sirens in the future. Such conclusion could also be derived through the comparison with other works by using different available SGL sub-

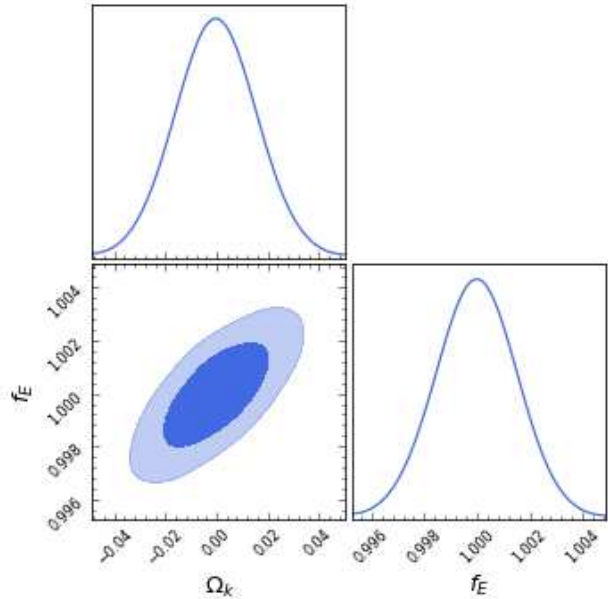


**Figure 4.** The 2-D regions and 1-D marginalized distribution with the  $1\sigma$  and  $2\sigma$  contours of all parameters, in the framework of SIS lens models.

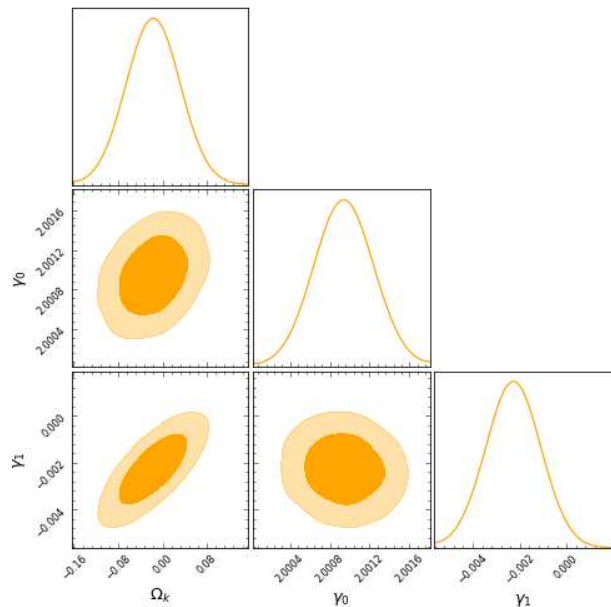


**Figure 5.** The 2-D regions and 1-D marginalized distribution with the  $1\sigma$  and  $2\sigma$  contours of all parameters, in the framework of power-law lens profile.

samples Xia et al. (2017); Qi et al. (2019a). In this analysis, the lens parameter characterizing the mass distribution profile  $f_E$  is also estimated in a global fitting without taking any prior. To study the correlation between  $\Omega_K$  and  $f_E$ , we display the two-dimensional (2D) probability distributions in the  $(\Omega_K, f_E)$  plane, with the marginalized  $1\sigma$  constraint of the parameter  $f_E = 1.000_{-0.002}^{+0.002}$ . It is interesting to note that our results, which strongly support a flat universe together with the validity of SIS model ( $\Omega_K = 0, f_E = 1$ ), reveal significant degeneracy

<sup>5</sup> <https://emcee.readthedocs.io/en/stable/>

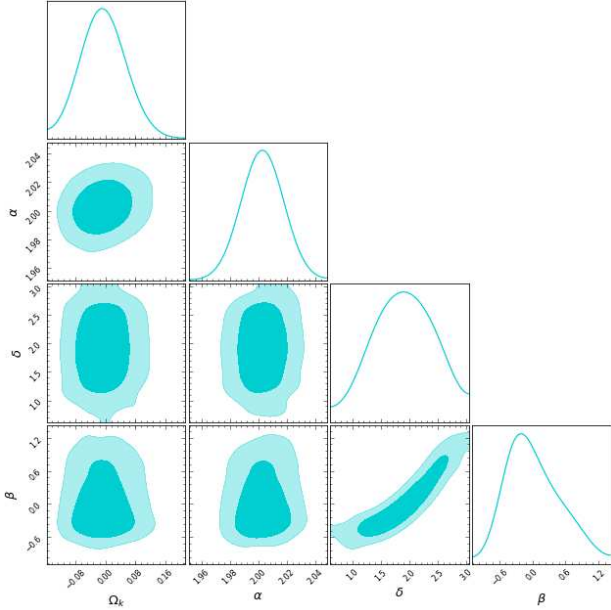


**Figure 6.** The 2-D regions and 1-D marginalized distribution with the 1- $\sigma$  and 2- $\sigma$  contours of all parameters, in the framework of extended power-law lens profile.

between the spatial curvature of the universe and the  $f_E$  parameter, which characterizes the mass distribution of the lensing galaxies. The numerical results are also summarized in Table 1.

Now we focus our attention on the constraints on the parameters in the framework of power-law mass density profile, in which the mass density power-law index of massive elliptical galaxies evolves with redshift ( $\gamma = \gamma_0 + \gamma_1 \times z_l$ ). Performing fits on the data comprising the strong lensing systems in LSST and the luminosity distance measurements from standard sirens in DECIGO, we obtain the following best-fit values and corresponding 1 $\sigma$  uncertainties:  $\Omega_K = -0.016^{+0.035}_{-0.037}$ ,  $\gamma_0 = 2.001^{+0.001}_{-0.001}$  and  $\gamma_1 = 0.002^{+0.003}_{-0.003}$ . The 1D and 2D marginalized distribution for  $\Omega_K$  and the power-law model parameters are shown in Fig. 5. It is turned out that the fit on the cosmic curvature in this case is still very strong compared with that found for the SIS model, which indicates that our findings are quite robust. Meanwhile, contour plots in Fig. 5 show that the degeneracies among the cosmic curvature and lens parameters ( $\gamma_0$ ) in power-law mass density profile are similar to that of the SIS model ( $f_E$ ). More specifically, it is easy to find from the  $\Omega_K - \gamma_1$  contour that  $\Omega_K$  is strongly correlated with  $\gamma_1$ , which indicates that a significant redshift evolution of the mass density power-law index will result in a larger cosmic curvature. Therefore, compared with the previous results focusing on a constant power-law lens index parameter (Zhou & Li 2020), our analysis reveals that the estimation of the spatial curvature is more sensitive to the measurement of its possible evolution with redshifts. Such conclusion, which has been suggested by Ruff et al. (2011), is also further supported by Sonnenfeld et al. (2013a) in a combined sample of lenses from SLACS, SL2S, and LSD. Therefore, additional observational information, such as dedicated follow-up imaging of the lensed images for

a sample of individual lenses is necessary in this case. Such high-cadence, high-resolution and multi-filter imaging could be technically obtained through frequent visits on Hubble telescope or smaller telescopes on the ground (Collett & Auger 2014; Wong et al. 2015).

Let us finally focus on the performance of the extended power-law lens model, in which the total density slope, luminosity density slope and the anisotropy of stellar velocity dispersion are taken as free parameters. The graphical and numerical results from the combined DECIGO+LSST data set are displayed in Fig. 6 and Table 1. The values listed in Table 1 show that the extended power-law lens model generates competitive constraints on the cosmic curvature ( $\Omega_K = -0.007^{+0.050}_{-0.047}$ ) comparable with the power-law mass density profile. This is inconsistent with the results presented in Xia et al. (2017), where they have used the similar lens model (without considering the effect of the anisotropy of stellar velocity dispersion) but adopted different combinations of available data in the EM domain. Compared with the SNe Ia standard candles, the advantage of DECIGO standard sirens is that larger number of GWs could be observed at much higher redshifts, which motivate us to calibrate the LSST strong lenses and investigate the cosmic curvature in the early universe. More interestingly, the extended power-law lens model is more suitable to estimate the mass distribution of baryonic matter and dark matter in the early-type galaxies. Compared with the previous observational constraints on the total-mass density profile (Cao et al. 2016; Xia et al. 2017; Chen et al. 2019), the combined LSST+DECIGO data will improve the constraints significantly ( $\alpha = 2.003^{+0.011}_{-0.011}$  with respect to current results, showing the high constraining power that can be reached by the forthcoming surveys. Furthermore, as can be seen in Fig. 6 the addition of DECIGO to the combination of LSST+DECIGO does improve the constraint on the luminosity density slope ( $\delta = 1.968^{+0.527}_{-0.516}$ ) and the anisotropy of the stellar velocity dispersion significantly ( $\beta = -0.067^{+0.605}_{-0.325}$ ). Such steeper luminosity density profile and nonzero stellar velocity anisotropy parameter are consistent with Cao et al. (2016); Zhou & Li (2020) and also with recent results of Illustris simulations (Xu et al. 2016), focusing on early-type galaxies with spherically symmetric density distributions. In this case, auxiliary data such as integral field unit (IFU) spectroscopic data, especially Adaptive optics (AO) IFU spectroscopy on 8-40m-class telescopes or AO imaging with slit spectroscopy (Hložek et al. 2019), could provide complementary information of  $\delta$  and  $\beta$  in the near future (Barnabè et al. 2013).

Finally, in order to demonstrate the advantage of the second-generation technology of space-borne GW detector, in Fig. 7 we compare the results of DECIGO with those obtained using the third-generation ground-based Einstein Telescope (ET)<sup>6</sup>. See Qi et al. (2019b) for detailed description of the simulation process based on ET. It should be noted that adding the information brought by such a space-based GW detector to the combination of LSST+DECIGO does improve the  $\Omega_K$  constraints significantly. More specifically, the cosmic curvature is

<sup>6</sup> The Einstein Telescope Project, <https://www.et-gw.eu/et/>

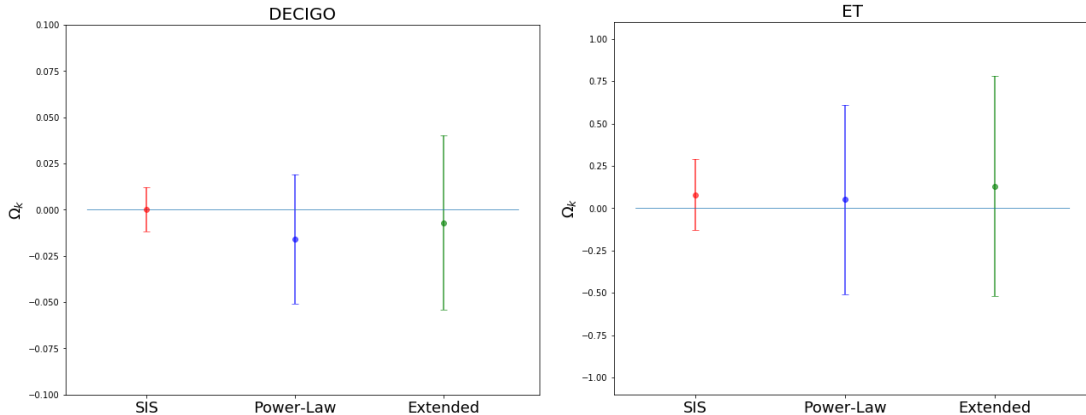


**Figure 7.** Determination of cosmic curvature with different GW detectors, future ground-based Einstein Telescope (ET) and satellite GW observatory (DECIGO).

expected to be constrained with an error smaller than  $10^{-2}$ , improving the sensitivity of ET constraints by about a factor of 10 in the framework of three kinds of spherically symmetric mass distributions (SIS, power-law model, and extended power-law model) for the lensing galaxies. Such conclusion could be not surprising, as although one would expect that ET would be ten times more sensitive than current advanced ground-based detectors, the neutron star-neutron star (NS-NS) mergers and black hole-neutron star (BH-NS) mergers systems could only be detected up to redshift  $z \sim 2$  and  $z \sim 5$ , respectively (Cai & Yang 2017). More importantly, benefit from the fundamentally self-calibrating capability of space-based detectors, the corresponding distance uncertainties for DECIGO may be reduced to 1 percent accuracy at lower frequencies (in the frequency range of 0.1-1 Hz) (Cutler & Holz 2009). This is to be compared with Fig. 1 in Qi et al. (2019b), whose forecast is for ET (with the specifications foreseen at the time) the luminosity distance measurements could be derived from 1000 observed GW events in the frequency range of  $1 - 10^4$  Hz. In summary, we do expect that the use of our technique, i.e., using luminosity distance of standard sirens detected by the second-generation technology of space-borne GW detector, would lead to a stronger improvement in the direct measurement of the spatial curvature in the early universe ( $z \sim 5.0$ ). However, in order to investigate this further, the mass density profiles of early-type galaxies should be properly taken into account (Qi et al. 2018).

## 5. CONCLUSIONS

The spatial curvature of the Universe has been one of the most important cosmological parameters in modern cosmology. Its value, or even its sign would help us rule out the standard cosmological paradigm or even point to the presence of new physics. In this work, we have quantified the ability of DECIGO, a future Japanese space gravitational-wave antenna in combination with galactic-scale strong lensing systems expected to be detected by LSST, to improve the current constraints on the cosmic curvature in the redshift range  $z \sim 5$ . In the framework of the well-known distance sum rule (Räsänen et al. 2015), the perfect redshift coverage of the standard sirens observed by DECIGO, compared with lensing observations including the source and lens from LSST, makes

such cosmological-model-independent test more natural and general. While we exploited a commonly used Singular Isothermal Ellipsoid (SIE) model to describe the mass distribution of lensing galaxies, we also use Power-law model and Extended power-law model to better assess the effect of lens model on measuring the cosmic curvature.

In the case of the simplest SIS lens model, due to the significant increase of well-measured strong lensing systems and standard sirens, one could expect the most stringent fits on the cosmic curvature which has been improved by two orders of magnitudes compared with the previous results obtained in Räsänen et al. (2015). Such precision is competitive with that derived from the Planck CMB power spectra (TT, TE, EE+lowP) data (Aghanim et al. 2018). For the second lens model, we have considered the power-law mass density profile in which the mass density power-law index of massive elliptical galaxies evolves with redshift. Our findings indicate that the constraint on the cosmic curvature in this case is still very strong compared with that found for the SIS model. However, our analysis reveals the strong degeneracy between the spatial curvature and the redshift evolution of power-law lens index parameter. Compared with the previous results focusing on a constant power-law slope, we show that the estimation of  $\Omega_K$  is more sensitive to the measurement of  $\gamma_1$ , i.e., a significant redshift evolution of the mass density power-law index will result in a larger cosmic curvature. Therefore, additional observational information, such as dedicated follow-up imaging of the lensed images for a sample of individual lenses is necessary in this case. Focusing on the performance of the extended power-law lens model, in which the total density slope, luminosity density slope and the anisotropy of stellar velocity dispersion are taken as free parameters, the combined LSST+DECIGO data will improve the constraints significantly with respect to current results, showing the high constraining power that can be reached by the forthcoming surveys. More interestingly, the extended power-law lens model is more suitable to estimate the mass distribution of baryonic matter and dark matter in the early-type galaxies. Specially, the addition of DECIGO to the combination of LSST+DECIGO does improve the constraint on the luminosity density slope and the anisotropy of the stellar velocity dispersion sig-



nificantly. In this case, our results highlight the importance of investigating the luminosity density slope and the anisotropy of the stellar velocity dispersion through auxiliary data, especially integral field unit (IFU) spectroscopic data in view of upcoming surveys.

What we are more concerned about is the advantage of higher quality data sets from the second-generation technology of space-borne GW detector, compared with the third-generation ground-based Einstein Telescope (ET). For this purpose, our analysis demonstrates that the cosmic curvature is expected to be constrained with an error smaller than  $10^{-2}$ , improving the sensitivity of ET constraints by about a factor of 10 in the framework of three kinds of lens models. In summary, our paper highlights the benefits of synergies between DECIGO and LSST in constraining the physical mechanism of cosmic acceleration or new physics beyond the standard model, which could manifest itself through accurate determination of the spatial curvature of the Universe.

This work was supported by National Key R&D Program of China No. 2017YFA0402600; the Ministry of Science and Technology National Basic Science Program (Project 973) under Grants No. 2014CB845806; the National Natural Science Foundation of China under Grants Nos. 12021003, 11690023, 11633001, and 11373014; Beijing Talents Fund of Organization Department of Beijing Municipal Committee of the CPC; the Strategic Priority Research Program of the Chinese Academy of Sciences, Grant No. XDB23000000; and the Interdiscipline Research Funds of Beijing Normal University. M.B. was supported by Foreign Talent Introducing Project and Special Fund Support of Foreign Knowledge Introducing Project in China. He is also grateful for support from Polish Ministry of Science and Higher Education through the grant DIR/WK/2018/12.

## REFERENCES

- Abbott, B. P., et al. 2016, PRL, 116, 061102  
 Abbott, B. P., et al. 2017, PRL, 119, 161101  
 Aghanim, N., Akrami, Y., Ashdown, M., et al. 2018, arXiv:1807.06209  
 Barnabè, M., et al. 2013, MNRAS, 436, 253  
 Bernstein, G. 2006, ApJ, 637, 598  
 Bolton, A. S., et al. 2012, ApJ, 757, 82  
 Bolton, A. S., et al. 2008, ApJ, 682, 964  
 Cai, R., Guo, Z., & Yang, T. 2016, PRD, 93, 043517  
 Cai, R.-G. & Yang, T. 2017, PRD, 95, 044024  
 Cao, S., Pan, Y., Biesiada, M., Godlowski, W., & Zhu Z.-H. 2012, JCAP, 03, 016  
 Cao, S., Biesiada, M., Gavazzi, R., Piórkowska, A., & Zhu, Z.-H. 2015b, ApJ, 806, 185  
 Cao, S., Biesiada, M., Yao, M., & Zhu, Z.-H. 2016, MNRAS, 461, 2192  
 Cao, S., et al. 2017, ApJ, 835, 92  
 Cao, S., et al. 2017, JCAP, 02, 012  
 Cao, S., et al. 2017, A&A, 606, A15  
 Cao, S., et al. 2018, ApJ, 867, 50  
 Cao, S., et al. 2019, NatSR, 9, 11608  
 Cao, S., et al. 2019, PRD, 100, 023530  
 Cao, S., et al. 2020, ApJL, 888, L25  
 Chen, Y., Li, R., Shu, Y. & Cao, X. 2019, MNRAS, 488, 3745  
 Choi, Y.-Y., Park, C., & Vogeley, M. S. 2007, ApJ, 884, 897  
 Clarkson, C., Cortes, M., & Bassett, B. 2007, JCAP, 08, 011  
 Clarkson, C., Bassett, B., Lu, T. H.-C. 2008, PRL, 101, 011301  
 Collett, T. E. & Auger, M. W. 2014, MNRAS, 443, 969  
 Collett, T. E. 2015, ApJ, 811, 20  
 Collett, T. E., & Cunningham, S. D. 2016, MNRAS, 462, 3255  
 Collett, T. E., et al. 2018, Science, 360, 1342  
 Cutler, C. & Harms, J. 2006, PRD, 73, 042001  
 Cutler, C. & Holz, D. E. 2009, PRD, 80, 104009  
 Denissenya, M., Linder, E. V., & Shafieloo, A. 2018, JCAP, 03, 041  
 Foreman-Mackey, D., Hogg, D. W., Lang, D., & Goodman, J. 2013, PASP, 125, 306  
 Frieman, J., & Dark Energy Survey Collaboration, 2004, BAAS, 36, 1462  
 Futamase, T., & Yoshida, S. 2001, PThPh, 105, 887  
 Geng, S., et al. 2020, ApJ, 905, 54  
 Gong, Y.-G., & Wang, A. 2007, PRD, 75, 043520  
 Hilbert, S., et al. 2009, A&A, 499, 31  
 Hložek, R. A., et al. arXiv:1903.09324  
 Humphrey, P. J., & Buote, D. A. 2010, MNRAS, 403, 2143  
 Ichikawa, K., et al. 2006, JCAP, 12, 005  
 Kawamura, S., Nakamura, T., Ando, M. et al., 2006, CQG, 23, 125  
 Kawamura, S., Nakamura, T., Ando, M. et al., 2019, IJMPD, 28, 1845001  
 Kawamura, S., et al. 2011, CGQ, 28, 094011  
 Koopmans, L. V. E. 2005, Proceedings of XX1st IAP Colloquium, (Paris, 4-9 July 2005), eds G. A. Mamon, F. Combes, C. Deffayet, B. Fort (Paris: EDP Sciences) [arXiv:0511121]  
 Koopmans, L. V. E., et al. 2006, ApJ, 649, 599  
 Li, X. L., et al. 2016, RAA, 16, 84  
 Li, Z.-X., Wang, G.-J., Liao, K., & Zhu, Z.-H. 2016, ApJ, 833, 240  
 Liu, T. H., et al. 2019, ApJ, 886, 94  
 Liu, T. H., et al. 2020, MNRAS, 496, 708  
 Ma, Y. B., et al. 2019, EPJC, 79, 121  
 Maggiore, M. Gravitational Waves, 2008, Oxford University Press, New York  
 Mandelbaum, R., et al. arXiv:1903.09323  
 Messenger, C. & Read, J. 2012, PRL, 108, 091101  
 Messenger, C., Takami, K., Gossan, S., Rezzolla, L., & Sathyaprakash, B. S. 2014, PRX, 4, 041004  
 Nishizawa, A., Taruya, A., & Kawamura, S. 2010, PRD, 81, 104043  
 Ofek, E. O., Rix, H. W., & Maoz, D. 2003, MNRAS, 343, 639  
 Oguri, M., & Marshall, P. J. 2010, MNRAS, 405, 2579  
 Ooba, J., Ratra, B., & Sugiyama, N. 2018, ApJ, 864, 80  
 Piórkowska-Kurpas, A., et al. 2020, ApJ, submitted [arXiv:2005.08727]  
 Qi, J.-Z., et al. 2018, RAA, 18, 66  
 Qi, J.-Z., et al. 2019a, MNRAS, 483, 1  
 Qi, J. Z., et al. 2019b, PRD, 99, 063507  
 Qi, J. Z., et al. 2019c, PDU, 26, 100338  
 Rana, A., Jain, D., Mahajan, S., & Mukherjee A. 2017, JCAP, 03, 028  
 Räsänen, S., et al. 2014, JCAP, 03, 035  
 Räsänen, S., Bolejko, K., & Finoguenov, A. 2015, PRL, 115, 101301  
 Ratra, B., & Peebles, P. E. J. 1988, PRD, 37, 3406  
 Risaliti, G., & Lusso, E. 2019, Nature Astronomy, 3, 272  
 Ryan, J., et al. 2019, arXiv:1902.03196  
 Ruff, A. J., et al. 2011, ApJ, 727, 96  
 Sathyaprakash, B., et al. 2010, CQG, 27, 215006  
 Schneider, R., et al. 2001, MNRAS, 324, 797  
 Seto, N., Kawamura, S., & Nakamura, T. 2001, PRL, 87, 221103  
 Schutz, B. F. 1986, Nature, 323, 310  
 Shafieloo, A., & Clarkson, C. 2010, PRD, 81, 083537  
 Sonnenfeld, A., et al. 2013a, ApJ, 777, 98  
 Sonnenfeld, A., Gavazzi, R., Suyu, S. H., Treu, T., & Marshall, P. J. 2013b, ApJ, 777, 97  
 Takada, M., & Doré, O., 2015, PRD, 92, 123518  
 Treu T., Koopmans L. V., Bolton A. S., Burles S., Moustakas L. A., 2006, ApJ, 640, 662  
 Verma, A., et al. 2019, arXiv:1902.05141  
 Virey, J. M., et al. 2008, JCAP, 12, 008  
 Wang, G.-J., et al. 2017, ApJ, 847, 45  
 Wei, J.-J., & Wu, X.-F. 2017, ApJ, 838, 160  
 Wong, K. C., Suyu, S. H., & Matsushita, S. 2015, ApJ, 811, 115  
 Xia, J.-Q., et al. 2017, ApJ, 834, 75  
 Xu, D. D., Springel, V., Sluse, D., et al. 2016, arXiv:1610.07605v1  
 Yagi, K. & Seto, N. 2011, PRD, 83, 044011  
 Zhang, S., et al. 2020, IJMPD, in press [arXiv:2009.04204]

Zhao, W., Van Den Broeck, C., Baskaran, D., & Li, T. 2011,  
PRD, 83, 023005

Zhou, H. & Li, Z. 2020, ApJ, 899, 186